Analysis of wake properties and meandering under different cases of atmospheric stability: a large eddy simulation study

Analysis of wake properties and meandering under different cases of atmospheric stability: a large eddy simulation study

Erwan Jézéquel [1,2], Frédéric Blondel[1], Valéry Masson[2]

[1]IFP Energies nouvelles, 1-4 Avenue de Bois Préau, Rueil-Malmaison, France.
[2]Centre National de Recherches Météorologiques, 42 avenue Gaspard Coriolis, Toulouse, France.

E-mail: erwan.jezequel@ifpen.fr

Abstract. Large eddy simulations (LES) with the solver Meso-NH are performed to analyse a single wind turbine wake. In the first part of this work, four algorithms to determine the instantaneous wake centre (wake tracking) from the literature are compared. A data-processing method is also proposed to improve the results of these algorithms. In the second part, three different atmospheric conditions are simulated to assess the effect of inflow conditions on the wake. The focus is on the 2-dimensional wake width, the maximum deficit, the maximum added turbulence and the amount of wake meandering in the lateral and vertical directions. The three formers are computed in both the Moving and Fixed Frames of Reference (MFOR and FFOR). Results in the MFOR are shown to be sensitive to the wake tracking algorithm, in particular for turbulence. The flowfield in the MFOR is found to be independent of atmospheric conditions for the two cases with similar operating conditions and length scales larger than two diameters of the rotor. The third case with lower length scales and turbulence intensity behaves differently.

1. Introduction

The wake behind a wind turbine is characterised by a lower wind velocity and a higher level of turbulent kinetic energy (TKE) compared to the inflow properties. The wind turbine wakes interact with the atmospheric boundary layer (ABL): the largest eddies of the ABL induce meandering, i.e. oscillations of the wake around its mean position [1], and the atmospheric stability modifies the wake recovery [2]. In order to study and optimise wind farm layouts, many analytical models for the velocity deficit have been proposed. This work is based on the bivariate gaussian shape [3]:

$$\Delta U(x,y,z) = C(x) e^{-\frac{y^2}{2\sigma_y(x)^2} - \frac{z^2}{2\sigma_z(x)^2}} \quad (1)$$

where $\Delta U = (\overline{U}_\infty - \overline{U})/\overline{U}_\infty$ is the mean, non-dimensional velocity deficit in the wake, with $\overline{U}_\infty$ the mean upstream velocity, σ_y, σ_z the lateral and the vertical wake widths and (x, y, z) the streamwise, lateral and vertical coordinates respectively. This gaussian shape of the velocity deficit can be found in the far wake i.e. for $x > 3D$ where D is the turbine diameter. Based on momentum conservation, $C(x)$ takes the following form [4]:

$$C(x) = 1 - \sqrt{1 - \frac{C_T}{8\sigma_y(x)\sigma_z(x)/D^2}} \tag{2}$$

where C_T is the thrust coefficient. Due to the blade bound vorticity, the shear generated by the velocity deficit and the wake meandering, the wake is also a region of increased TKE [5]. Most analytical models dealing with turbulence in wakes are empirical and focus on the streamwise evolution of the maximum added TKE [3, 6], possibly modulated by a shape function [7].

When computing the mean and variance of the wake velocity field over a time period larger than the meandering period, the wake is spread on the meandering range. Consequently, the wake deficit is lower, and its width larger compared to a non-meandering wake. In order to decouple the 'natural' expansion of the wake and the effect of meandering, it is here proposed to work with the Moving and Fixed Frames of References (MFOR and FFOR, respectively), as in the Dynamic Wake Meandering model (DWM) [1]. The latter is linked to the ground: it is the frame of reference of the simulation. The former is moving with the wake centre at each timestep. The wake behaves in the MFOR as if there is no meandering: the mean velocity deficit is higher and narrower than in the FFOR because it is not spread by meandering. Conversely, it has been measured that the streamwise turbulence is lower than in FFOR [8], which can be attributed to the absence of meandering turbulence in the MFOR.

To compute the velocity in the MFOR, the position of the wake centre at each timestep must be found (this is called 'wake tracking' in the following). The first objective of this work is to compare the reliability of different tracking algorithms and to show that the choice of the algorithm induces important changes in the resulting mean and turbulence fields in the MFOR. A pre-processing method is also proposed to improve the tracking. Previous works have shown, with a simpler tracking algorithm, that the atmospheric stability strongly affects the wake meandering but has a minor impact on the mean wake velocity in the MFOR [9, 10, 11]. The second objective of this work is to verify this observation with a more reliable algorithm and a new set of data. The improved reliability of the presented wake tracking allows to study the turbulence field in the MFOR between from $x/D = 1$ to $x/D = 8$ and its dependency on atmospheric stability (extending the work of [12] that was restrained to $x = 2.5D$). Understanding the behaviour of TKE in the MFOR is an important step towards physically-based models of TKE that take into account meandering, either dynamically as in the DWM model or analytically [13].

2. Numerical simulation

2.1. The SWiFT cases

This study is based on numerical simulations reproducing the SWiFT benchmark [10] where several codes were compared to *in-situ* measurements of a single utility-scale wind turbine of diameter $D = 27$ m and hub height $z_{hub} = 32.1$ m, located in a flat terrain. Three cases are studied: near-neutral, unstable and strongly stable. In the simulations, the stability parameter at $z = 10$ m is respectively $z/L_{MO} = \{0.003, -0.159, 0.601\}$ where L_{MO} is the Monin-Obukhov length, the inflow velocity at hub height is $U = \{8.4, 6.2, 3.7\}$ m/s, the inflow streamwise turbulence intensity (TI) at hub height is $TI_x = \{11.2, 12.3, 4.7\}\%$ and the thrust coefficient is $C_T = \{0.79, 0.81, 0.82\}$. Inflow conditions, turbine response and time-averaged velocity deficit of Meso-NH have already been presented in a previous work [14], so here the focus is on the meandering properties and on the wake in the MFOR and the FFOR.

2.2. The Meso-NH LES solver

These three cases are simulated with the LES solver Meso-NH [15]. The aneslatic (a constant density profile $\rho(z)$ is imposed, excepted for the buoyancy term) and non-hydrostatic (the vertical velocity is driven by the vertical pressure gradient and the gravity) Navier-Stokes equations along with the energy conservation equation are resolved with a finite volume method on an Arakawa grid. The unknowns are the 3-D velocity components (U_x, U_y and U_z) and the potential temperature θ. The momentum equation takes into account buoyancy, the Coriolis force and large-scale forcing. The latter is written as a 2-D geostrophic wind that is imposed by the user.

An equation for the subgrid kinetic energy e_{sgs} and a mixing length L_m are introduced for the turbulence closure. The subgrid terms are written as a function of e_{sgs}, L_m and the resolved terms [16]. The mixing length is related to the grid size and stratification through the Deardorff formulation [17]. A fourth-order centred scheme and a fourth-order Runge-Kunta scheme are used for spatial and temporal discretisation. To model the wind turbine, the actuator line method (ALM) is used, following [18]. The implementation in Meso-NH has been validated against the NewMexico experiments [19] and the SWiFT benchmark [14].

2.3. Numerical parameters

In order to initialise the neutral and unstable ABL, a first domain D_1 is created, with streamwise and transverse dimensions of 6 km $\times$ 2.4 km and 12 km $\times$ 6 km respectively, and a coarse horizontal mesh width of 20 m. The flowfield is initialised with a constant-velocity profile equal to the geostrophic wind and a constant-temperature profile up to 1000 m, capped by an inversion region (5K/50m). To go down in resolution, a nesting is performed: the flowfield of D_1 in a given region is used as the boundary conditions of a new domain D_2, of smaller dimensions and finer mesh [20]. This operation is repeated twice in order to reach 0.5 m resolution i.e. about 60 mesh points per rotor diameter as recommended in [21]. In each nested domain, a turbulence build-up region (in brown in Figure 1) appears near the inflow, where the flowfield is not physically realistic. For the stable case, the same procedure is used but since the largest eddies are much smaller, the dimensions of D_1 are reduced to 630 m $\times$ 350 m long and wide, its horizontal resolution is 1.2 m and the ABL height is 200 m. Only one nesting is necessary to reach 0.4 m resolution.

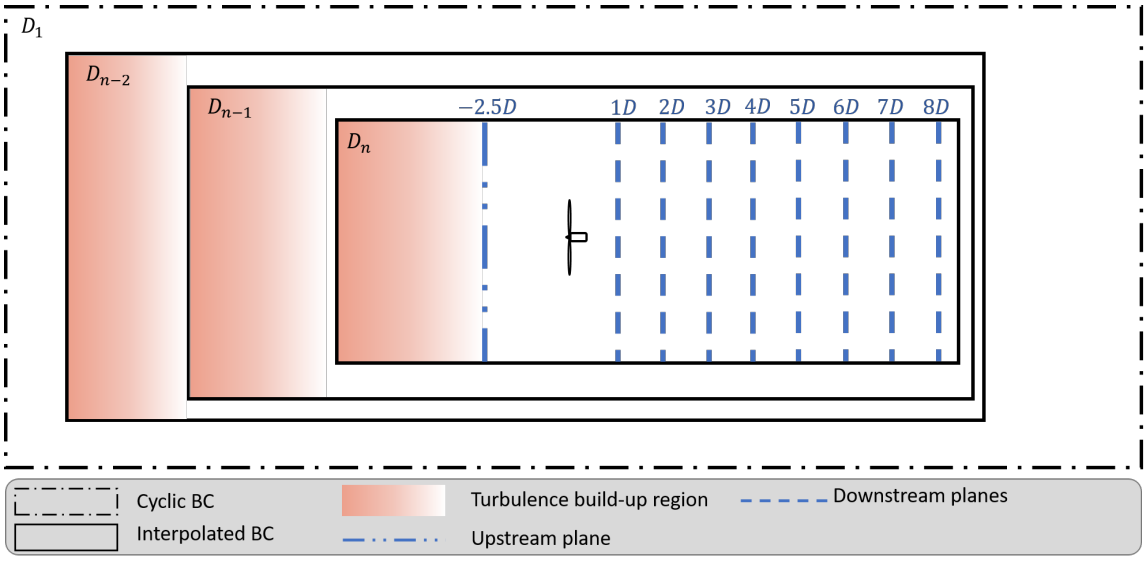

Figure 1. Schematic of the simulation set-up with Meso-NH.

The vertical mesh is the same for every domain and is set to have isotropic cells in the most refined domain from the ground to the top tip of the turbine. Prescribed surface roughness and ground heat flux are used to build a bottom boundary condition for the temperature and velocity through the Monin-Obukhov similarity theory. Once the flowfield is initialised in the most refined model, the ALM is activated with imposed constant rotational velocity and blade pitch, deduced from the characteristics of the SWiFT turbine. A simple implementation of the nacelle and the tower is used (following [22]). After a 10-minutes spin-up to let the flow establish, the instantaneous velocities are extracted at 1 Hz for one plane $-2.5D$ upwind the turbine and planes downwind from $1D$ to $8D$ (see Figure 1). Statistics are then computed over the whole simulation, i.e. 80 min, 40 min and 10 min for the neutral, unstable and stable cases respectively.

3. Wake tracking

3.1. Context

In order to compute the amount of meandering and the velocity field in the MFOR, it is necessary to determine the wake centre position at each timestep, hereafter noted $y_c(t), z_c(t)$ for the horizontal and vertical coordinates. The most common wake-tracking algorithm (abbreviated Gauss2D) consists in fitting a 2D-gaussian function on the instantaneous, non-normalised velocity deficit field $\delta U = U(x, y, z, t) - U_0$ where U_0 is the unperturbed velocity (detailed later). In another algorithm (denoted MinPower), the wake centre is defined as the region with the lowest available power [23], i.e. a minimisation algorithm is applied at every time step on the function:

$$f(y_c, z_c) = \int\int_{S_T} U^3(y - y_c, z - z_c) dy dz \tag{3}$$

where S_T is a disk of the size of the rotor-swept area. In a third method (denoted CstArea), the wake outline is deduced from a δU isoline enclosing an area S equal to the rotor-swept area. This algorithm can instead be based on the momentum conservation (it is then denoted CstFlux) i.e. the wake outline is computed as a δU isoline enclosing a surface S such as:

$$\rho \int\int_S U \left[U_0 - U\right] dS = \overline{T} \tag{4}$$

where ρ the density of the fluid and $\overline{T}$ is the mean thrust [24]. In the CstArea and CstFlux algorithms, the wake centre is then computed as the velocity deficit centroid of S. The four algorithms are applied to the extracted instantaneous velocity planes from Meso-NH with the SAMWICH python toolbox (used in [10, 24, 25]). Each algorithm can lead to erroneous wake centre computation: low-speed eddies of the ABL can be 'mistaken' with the wake and turbulence tends to modify the wake shape, or even split it, making it hardly detectable.

In the literature, the unperturbed velocity is often defined as the *Upstream* velocity, i.e. $U_0(z) = \overline{U}_\infty(z)$ (here taken in the plane at $x = -2.5D$), allowing to remove the mean shear but not the instantaneous eddies of the ABL. Instead, it is here proposed to use instantaneous velocity planes from a *Reference* simulation, which is another LES simulation with the same boundary conditions and inflow but without the turbine: $U_0 = U_{ref}(x, y, z, t)$. The eddies of the ABL not affected by the wake are the same in both simulations and should be cancelled when subtracting $U - U_0$. This method is computationally more expensive as it requires running another LES simulation.

To smooth the field on which tracking algorithms are applied, a moving average operator $< . >$ can be applied to the velocity and reference velocity fields, as in [26]:

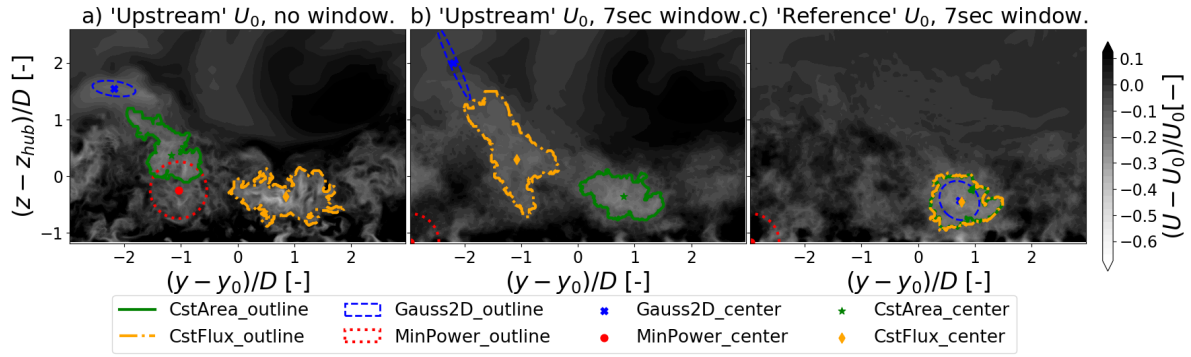

Figure 2. Results of different wake tracking strategies for the frame 199s at x/D=8.

$$< U > (t) = \frac{1}{\delta t} \int_{t-\delta t/2}^{t+\delta t/2} U(\tau) d\tau \tag{5}$$

where δt is the window size. One must take care that the meandering motions are not filtered out by doing so. When the power spectral density of y_c is computed as a function of the frequency, it appears that most of the variance of y_c is coming from frequencies lower than $U_c/4D \approx 0.13$ Hz $\approx 1/7$ Hz. U_c is the convection velocity of the large scales of the wake, which is here set to $0.8 \cdot U_\infty$, according to wind tunnel measurements [27]. The window size is thus set to $\delta t = 7$ seconds to ensure that the meandering process of the wake is only marginally affected by the time-averaging procedure.

3.2. Results

The efficiency of the four tracking algorithms as well as of the pre-processing methods are assessed on the neutral case. The four tracking algorithms are tested on the velocity deficit field defined by: the *Upstream* definition without moving average (Figure 2a), the *Upstream* definition with moving average (Figure 2b) and the *Reference* definition with moving average (Figure 2c). Figure 2 shows on purpose a case ($x/D = 8$ at $t = 199$ s) where the differences are strong and the wake centre is not trivial to identify. In Figures 2a and 2b, two regions of low-velocity are present, one near $y/D = 1$ and the other near $y/D = -1$, which can both potentially be the wake, leading the algorithms CstArea and CstFlux to find different results. For this particular frame, using the *Reference* unperturbed velocity along with the moving average (Figure 2c) allows to solve the ambiguity and define the wake position as the one located at $y/D = 1$.

	Upstream			Reference			
total	Gauss2D	CstArea	CstFlux	Gauss2D	CstArea	CstFlux	Ambiguous
400	79	39	37	53	43	14	20
%	19,75	9,75	9,25	13,25	10,75	3,5	5
AutomDetec	40	0	0	31	0	0	
Remaining(%)	9,75	9,75	9,25	5,5	10,75	3,5	

Table 1. Number of errors for different wake tracking strategies at $x/D = 8$ for the first 400 frames.

To compare the tracking algorithms, results for the first 400 frames at $x/D = 8$ for the two definitions of U_0 have been visually checked. For each algorithm, the number of timesteps

where the output wake position is wrong is reported in Table 1. No criteria could be found to characterise automatically whether the algorithm failed or not so this visually-based method is the best at our disposal. This qualitative analysis is based on whether the minimum velocity (excluding the small eddies attached to the ground) is included in the detected wake, and on the coherence of the studied frame with the precedent and succeeding frames. In some situations (5% of the studied frames), it is difficult to determine which algorithm is predicting the actual wake centre: these are noted as *Ambiguous* frames and not counted in the other columns of Table 1.

Results without the moving average or with the MinPower algorithm are not shown due to too many outliers. For both U_0 definitions, the Gauss2D algorithm leads to the highest number of errors, followed by CstArea and then CstFlux. The *Reference* definition of unperturbed velocity allows to reduce this number for the Gauss2D and CstFlux methods. It is possible to automatically detect about half the errors of the Gauss2D algorithm by discarding the wake centre position detected near the edges of the frames, making it as reliable as the CstArea algorithm in term of number of errors. However recovering the wake centre at these timesteps from interpolation is prone to errors because they tend to appear on several frames in a row, leading to about 10% missing data. Consequently, the CstFlux algorithm with the *Reference* definition of U_0 is considered the one working the best with only 3.5% of errors.

3.3. Impact on the MFOR

To compute the instantaneous velocity field in the MFOR, the velocity field in the FFOR is interpolated at each time step:

$$U_{MFOR}(x, y_{MFOR}, z_{MFOR}, t) = U_{FFOR}(x, y_{FFOR} + y_c(t), z_{FFOR} + z_c(t), t). \tag{6}$$

Given that the ground is located around $z_{FFOR} \approx -1.2D$ and that the minimum value of z_{MFOR} is set to $-1D$, then for the frames where $z_c(t) < -0.2D$, the velocity field at $U_{MFOR}(z_{MFOR} < -1.2D - z_c(t))$ is located under the ground and is thus undefined. Since extrapolation led to erroneous results, these values are ignored when computing the mean velocity and TKE in the MFOR. It should also be noted here that only the streamwise velocity field U_x is computed in the MFOR so only the corresponding component of the TKE $k_x = \overline{u'u'}$ is studied. Since the data have been sampled at 1 Hz, the values of k_x presented herein do not include the variations of higher frequency nor the subgrid-scale turbulence.

The lateral profiles (taken at hub height) of $-\Delta U_x$ and k_x at $x/D = 8$ are plotted in Figure 3 for the Gauss2D and CstFlux algorithms, with the two definitions of U_0 for the tracking. The impact of the moving average has been observed to be small and is thus not shown here. The different tracking strategies result up to 20% difference for the maximum velocity deficit, which is non-negligible. Overall, using the Gauss2D and *Upstream* lead to stronger deficit than using CstFlux and *Reference*. Secondly, the k_x predicted from the *Reference* definition of U_0 has a more realistic shape than the one predicted with the *Upstream* definition, i.e. a symmetric profile with respect to $y = 0$ and with values approaching the inflow turbulence $k_{x,\infty}$ for $y \to \pm\infty$. Three interpretations for the values of $k_x < k_{x,\infty}$ are proposed, that have not been yet been verified by the authors:

- Since the MFOR is 'following' the largest eddies of the atmosphere, the variability of these eddies are not taken into account. According to the DWM theory, only the length scales lower than $U/2D$ should be taken into account to compute the upstream TKE in the MFOR. This interpretation would also explain why this phenomenon is not observed in the stable case where even the largest turbulence scales are lower than $2D$.
- Here only the streamwise component of the TKE is taken into account. A possible interpretation would be that there is a redistribution between $\overline{u'u'}$, $\overline{v'v'}$ and $\overline{w'w'}$ that

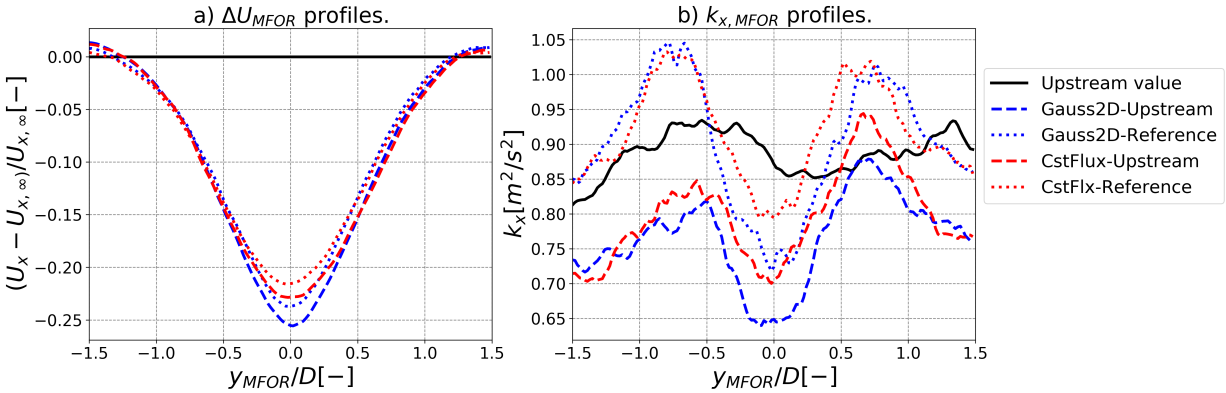

Figure 3. Impact of the wake tracking algorithm on the velocity deficit and turbulence profiles in the MFOR for the neutral case at $x/D = 8$.

leads to lower values of $k_x = \overline{u'u'}$ in some regions of the wake. The analysis of the lateral and vertical components of the velocity field in the MFOR could validate this interpretation, but it is not clear to the authors whether or not a Galilean [8] transformation should be applied to these components before looking at such TKE budget.

- Finally, the wake tracking sensibility should be underlined. Since no perfect tracking strategy has been proposed yet, the errors necessarily propagate to the computation of the TKE. However, it cannot be the only source since negative values of Δk_{MFOR} are observed at $x/D = 1$ where there are almost no errors.

4. Influence of the atmospheric stability.

The preceding part showed that the best results of wake tracking are obtained with the CstFlux algorithm, applied with the *Reference* definition of U_0, smoothed with a moving averaged operator with $\delta t = 7$ s. In the following, this will be used to compute the time series $y_c(t), z_c(t)$ for the three cases of stability defined in section 2.1 to determine the effect of stability on the amount of meandering and wake properties in the MFOR and FFOR.

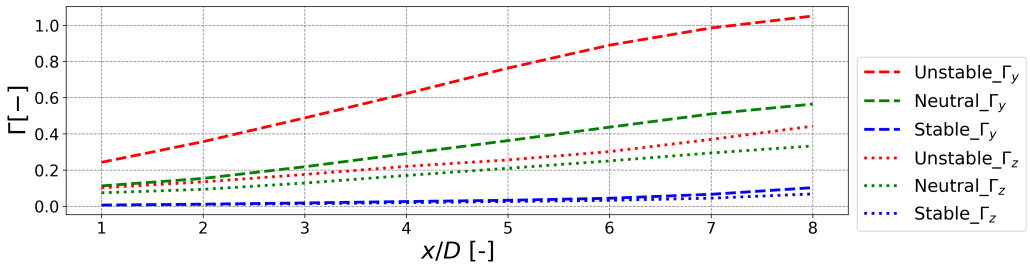

Figure 4. Amount of wake meandering in the vertical and horizontal directions.

4.1. Wake meandering.

The amount of meandering Γ is computed as the standard deviation of the wake centre position normalised by the turbine diameter:

$$\Gamma_y = \sqrt{\overline{y_c'^2}^d}/D \tag{7}$$

where exponent d indicates that the linear trend of the signal has been removed. It is plotted as a function of x/D for both directions (dashed lines for lateral direction and dotted lines for vertical direction) in Figure 4. In all the following, the colours red, green and blue stand for the unstable, neutral and stable cases, respectively. Similarly to other LES studies, the horizontal meandering is stronger than the vertical one and the stronger the stability, the weaker the meandering. Since the inflow streamwise turbulence of the neutral and unstable cases are similar, it cannot be a pertinent parameter to estimate the amount of meandering.

One can also note that the anisotropy of the wake meandering, characterised by the ratio Γ_y/Γ_z, takes values between 2.5 and 3 for the unstable case, around 1.75 for the neutral case and around 1.25 for the stable case. Other LES studies have shown similar behaviour of decreasing anisotropy with increasing stability [2, 11], whereas the opposite trend has been observed in full-scale lidar measurements [12]. It must be noted that the turbine and atmospheric conditions vary from one study to another and that all these studies use a gaussian-fit algorithm of wake tracking which produces more errors. More work is thus needed before concluding on wake meandering anisotropy.

4.2. Velocity deficit.

In order to quantify the wake expansion, which is crucial to derive a MFOR-based wake model, the following function is fitted to the mean 2D-velocity deficit ΔU for the three cases of stability and in the MFOR and FFOR:

$$f(y,z,C_0,y_0,z_0,\sigma_y,\sigma_z,\omega) = C_0 + Ce^{-a(y-y_0)^2-2b(y-y_0)(z-z_0)-c(z-z_0)^2} \tag{8}$$

with $a = \left(\frac{cos^2\omega}{2\sigma_y^2} + \frac{sin^2\omega}{2\sigma_z^2}\right)$, $b = \left(-\frac{sin2\omega}{4\sigma_y^2} + \frac{sin2\omega}{4\sigma_z^2}\right)$ and $c = \left(\frac{sin^2\omega}{2\sigma_y^2} + \frac{cos^2\omega}{2\sigma_z^2}\right)$.

Parameter C is fixed as in Equation 2, and the optimisation is run on parameters $\{C_0, y_0, z_0, \sigma_y, \sigma_z, \omega\}$ where ω is the angle of rotation of the wake. The resulting σ_y and σ_z are plotted in Figure 5a and 5b respectively, in the FFOR (dashed lines) and MFOR (dotted lines). The value of ϵ as defined in [4] is also plotted in continuous lines.

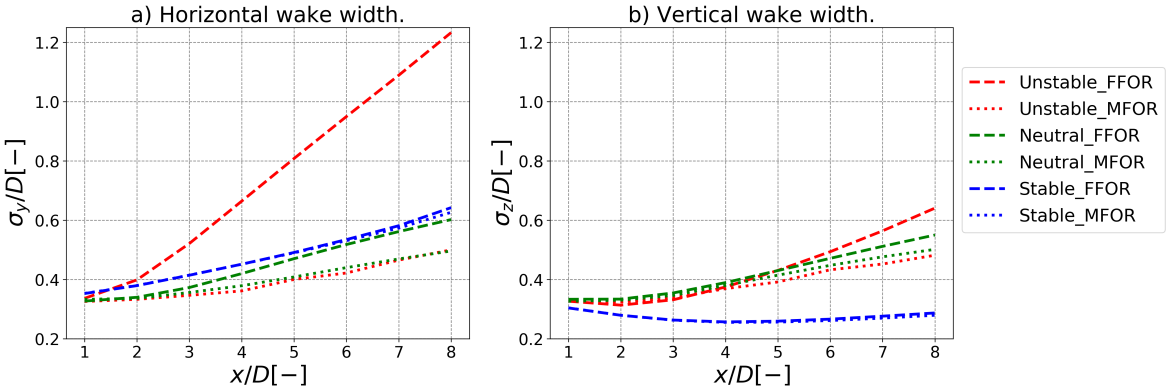

Figure 5. Evolution of the wake widths with x in both frames and for both directions.

For all cases and both frames of reference, the wake widths depend linearly on x/D, according to [4] and unlike bluff bodies wakes where $\sigma \sim x^{1/3}$. This linear relation is valid from $x/D = 3$ in the MFOR and $x/D = 2$ in the FFOR. Similarly to other works on stable ABL [28, 29], the wake in the stable case is skewed by an angle of about $\omega \approx 45°$ due to the strong veer. The induced deformation leads the wake to be elongated in one transverse direction and narrow in the perpendicular direction. The rotation parameter ω introduced in Equation 8, allows detecting

this deformation, making σ_y and σ_z no longer aligned with y and z but rather with the elongated and thin directions, respectively. It leads to the results plotted in Figure 5 where σ_y increases and σ_z is almost constant. Alternatively, one can compute σ_y and σ_z aligned with y and z by using a gaussian fit on 1D-profiles at $y = 0$ and $z = z_{hub}$ [2]. This latter methodology led to $\sigma_y \approx \sigma_z$ in the cited work but it is less straightforward to rebuild 2D velocity-deficit maps (e.g. for an analytical model) from such data than from rotated σ_y and σ_z and ω. Alternatively, the model developed in [28] could be used as a fitting function instead of Equation 8.

For the neutral and unstable cases in the MFOR, the wake width is fairly axisymmetric (dotted red and green lines are similar in Figures 5a and 5b), as it is assumed in the DWM [5]. Moreover, despite strong differences in the FFOR, the wake widths in the MFOR are equal in the neutral and unstable cases which could be due to similar values of C_T and $TI_{x,\infty}$ in the simulations, and thus the differences in the FFOR could be interpreted as being mainly due to different values of meandering. Finally, one can note that if $\sqrt{\sigma_y \sigma_z}$ was plotted, the stable case would be similar to the two other cases in the MFOR.

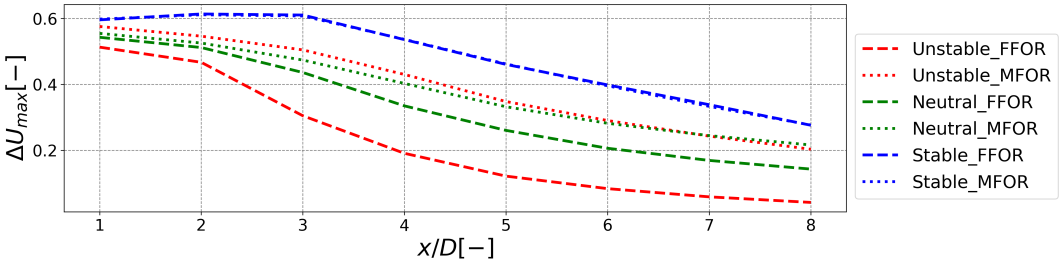

Figure 6. Maximum values of velocity deficit as a function of the downstream distance in both frames of reference.

The maximum absolute values of the wake deficit are plotted as a function of x/D in Figure 6 in the FFOR (dashed lines) and MFOR (dotted lines). The stronger the stability, the weaker the meandering (see Figure 4) and thus the smaller the difference between FFOR and MFOR. Moreover, the similarity of the velocity deficit between the neutral and unstable cases in the MFOR is again underlined on this graph, whereas in the FFOR they largely differ.

4.3. Added turbulence.
The streamwise added TI is hereby defined as:

$$\Delta TI(x,y,z) = \frac{\sqrt{\overline{u'^2}(x=-2.5D,y,z) - \overline{u'^2}(x,y,z)}}{U_h} \tag{9}$$

where U_h is the velocity at hub height. The value of ΔTI at the top tip ($z = D/2$) is plotted in Figure 7a as a function of x/D with the same plotting convention as above. In the MFOR, the TI at the top tip is similar between the neutral and unstable cases: it reaches a maximum at $x = 2D$ and then decreases somewhat linearly between $2D$ and $8D$. In the stable case, a plateau can be observed between $2D$ and $5D$ before the decrease, leading the top tip TI in the far wake to be greater in the stable case compared to the unstable and neutral cases. The same observations can be drawn in the FFOR at the difference that values are considerably larger (due to meandering turbulence) and that the maximum is reached about $1D$ upstream than in the MFOR. With comparable thrust coefficients and inflow turbulence intensities (but without thermal effects), similar amplitude and shape of the added turbulence at the top tip in the MFOR were found in [7] (see Figure 17, case 8 for the neutral and unstable cases and case 6 for the stable case).

The evolution of the maximum added TI in the wake (whatever is its position on each y-z plane) as a function of x is plotted in Figure 7b. It is confirmed from this second figure that in the MFOR, the flowfields of the unstable and neutral are still very similar one to another. From Figure 7a, one could conclude that the turbulence in the FFOR is similar between the unstable and neutral cases in the FFOR. However, the neutral TI profile takes a double-gaussian shape centred at the top tip in the neutral case whereas, due to the strong meandering, it quickly evolves to a simple-gaussian shape centred at hub height in the unstable case. Consequently, the top tip added TI is close to the maximum added TI in the neutral case, whereas it is not in the unstable case. Similarly, the maximum added TI in the stable case is displaced towards the negative y due to veer and is thus not captured by the value at the top tip.

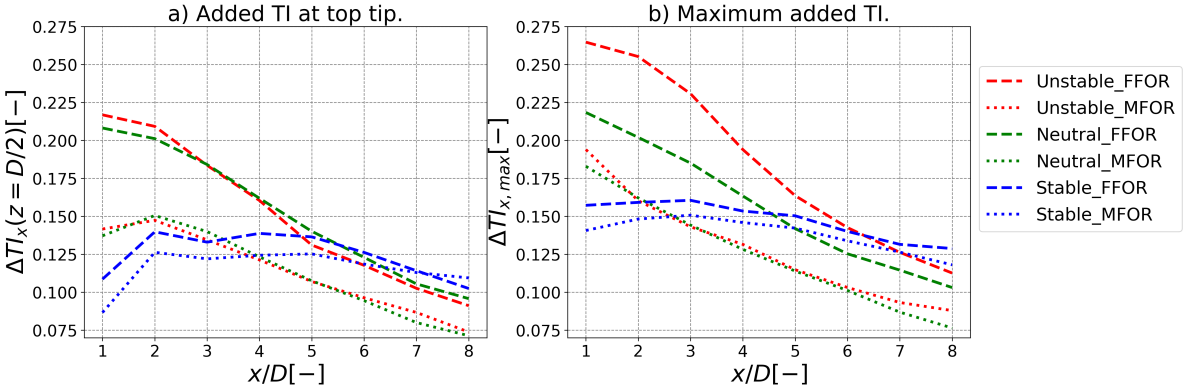

Figure 7. Maximum and top-tip values of the added turbulence intensity as a function of the downstream distance in both frames of reference.

Besides its different TI, the inflow of the stable case also differs from its spectral characteristics. The integral length scale L_x of the incoming flowfield has been investigated for the three cases of stability and compared to the cutoff length scale ($2D = 54$ m) used in the DWM to differentiate the eddies affecting the MFOR and the eddies affecting the meandering [1]. To do so, the integral timescale has been computed by integrating the auto-correlation of u' up to its first zero-crossing value. The product of this integral timescale with U_h leads to $L_x = \{335, 125, 15\}$ m i.e. $L_x/D = \{12.4, 7.6, 0.5\}$ for the unstable, neutral and stable cases respectively. Since $L_x < 2D$, there are almost no eddies energetic enough to move the whole wake in the stable case, explaining the very low values of Γ in Figure 4. Conversely, L_x is larger in the unstable case than in the neutral one, resulting in more meandering despite similar streamwise inflow TI (confirming the work of [11]).

Furthermore, the MFOR turbulence field in the stable case misses the eddies of size ranging between $L_x = 15$ m and $2D$, because such length scales do not exist in the inflow. This can be a secondary explanation for the differences in the MFOR with the neutral and unstable cases (see Figure 7) where all the length scales from the Kolmogorov scale to $2D$ are available in the inflow and will be found in the MFOR. According to this interpretation and if similar turbine operating conditions are met, a less-stable ABL would behave similarly to the neutral and unstable cases in the MFOR if $L_x > 2D$ in its inflow, and a more-unstable ABL would simply result in more meandering but similar flow in the MFOR. Even though three simulations are not enough to draw final conclusions, it confirms that the flow in the MFOR is mostly independent of atmospheric conditions, but shows that this assumption is not true where $L_x < 2D$. For small rotors like the Vestas V27, only strongly stable ABL fulfil this condition, but for very large rotors it could happen in more common atmospheric conditions.

5. Conclusions

This work aims at studying the wake of a single utility-scale wind turbine under different atmospheric conditions with the LES code Meso-NH. The first part focuses on different methodologies to find the time series of wake centre position. Four wake tracking algorithms are compared and a new definition of the unperturbed velocity used in the tracking algorithms is proposed, where the unsteady velocity of a *Reference* simulation with no turbine is used instead of the mean inflow velocity profile. It is shown that the choice of a wake tracking algorithm has an important impact on the velocity deficit and added turbulence in the MFOR. From the results presented in this study, it appears that the "CstFlux" algorithm (application of the momentum conservation) with the *Reference* definition of the unperturbed velocity works the best.

In the second part of this work, an analysis of the wind turbine wake in both frames of reference has been performed for three cases of atmospheric stability: unstable, neutral and strongly stable. The hypothesis of axisymmetric wake in the MFOR is validated for the neutral and unstable cases but not in the stable case where the strong veer of the ABL leads to a skewed wake. It is shown that for two cases where C_T and TI_x are similar (neutral and unstable), and despite very different results in the FFOR, a robust wake tracking leads to case-independent turbulence and velocity fields in the MFOR. Conversely, the wake in the stable case shows a very different behaviour, even in the MFOR, indicating a change of regime depending on atmospheric stability or turbulent intensity. These results are given for three specific atmospheric conditions and operating conditions and do not allow to conclude for all possible conditions of C_T, L_{MO}, U_∞ and TI. To do so quantitatively, a sensibility study on these parameters will be performed in future works to evaluate the impact on the MFOR and FFOR.

Acknowledgements

The authors would like to thank E. W. Quon for his work on wake tracking and the development of the SAMWICH python toolbox that was used in this work to compare the different tracking algorithms.

References

[1] Larsen G C, Madsen H A, Thomsen K and Larsen T J Wake meandering: a pragmatic approach 2008 *Wind Energy* **11** 377–395
[2] Abkar M and Porté-Agel F Influence of atmospheric stability on wind-turbine wakes: A large-eddy simulation study 2015 *Physics of Fluids* **27** 035104
[3] Xie S and Archer C Self-similarity and turbulence characteristics of wind turbine wakes via large-eddy simulation 2014 *Wind Energy* **18** 1815–1838
[4] Bastankhah M and Porté-Agel F A new analytical model for wind-turbine wakes 2014 *Renewable Energy* **70** 116–123
[5] Larsen G C, Madsen Aagaard H, Bingöl F, Mann J, Ott S, Sørensen J N, Okulov V, Troldborg N, Nielsen N M *et al.* 2007 *Dynamic wake meandering modeling* (Risø National Laboratory) ISBN 978-87-550-3602-4
[6] Frandsen S 2007 *Turbulence and turbulence-generated structural loading in wind turbine clusters* Ph.D. thesis DTU risø-R-1188(EN)
[7] Ishihara T and Qian G W A new Gaussian-based analytical wake model for wind turbines considering ambient turbulence intensities and thrust coefficient effects 2018 *Journal of Wind Engineering and Industrial Aerodynamics* **177** 275–292
[8] Larsen G, Pedersen A, Hansen K, Larsen T, Courtney M and Sjöholm M Full-scale 3d remote sensing of wake turbulence - a taster 2019 *Journal of Physics: Conference Series* **1256** 012001
[9] Machefaux E, Larsen G C, Koblitz T, Troldborg N, Kelly M C, Chougule A, Hansen K S and Rodrigo J S An experimental and numerical study of the atmospheric stability impact on wind turbine wakes 2015 *Wind Energy* **19** 1785–1805
[10] Doubrawa P, Quon E W, Martinez-Tossas L A, Shaler K, Debnath M, Hamilton N, Herges T G, Maniaci D, Kelley C L *et al.* Multimodel validation of single wakes in neutral and stratified atmospheric conditions 2020 *Wind Energy*
[11] Du B, Ge M, Zeng C, Cui G and Liu Y Influence of atmospheric stability on wind turbine wakes with a certain hub-height turbulence intensity 2021 *Physics of Fluids*

[12] Conti D, Dimitrov N, Peña A and Herges T Wind turbine wake characterization using the SpinnerLidar measurements 2020 *Journal of Physics: Conference Series* **1618** 062040
[13] Braunbehrens R and Segalini A A statistical model for wake meandering behind wind turbines 2019 *Journal of Wind Engineering and Industrial Aerodynamics* **193** 103954
[14] Jézéquel E, Cathelain M, Masson V and Blondel F Validation of wind turbine wakes modelled by the meso-NH LES solver under different cases of stability 2021 *Journal of Physics: Conference Series* **1934** 012003
[15] Lac C, Chaboureau J P, Masson V, Pinty J P, Tulet P, Escobar J, Leriche M, Barthe C, Aouizerats B *et al.* Overview of the meso-NH model version 5.4 and its applications 2018 *Geoscientific Model Development* **11** 1929–1969
[16] Cuxart J, Bougeault P and Redelsperger J L A turbulence scheme allowing for mesoscale and large-eddy simulations 2000 *Quarterly Journal of the Royal Meteorological Society* **126** 1–30
[17] Deardorff J W Stratocumulus-capped mixed layers derived from a three-dimensional model 1980 *Boundary-Layer Meteorology* **18** 495–527
[18] Sørensen J N and Shen W Z Numerical modeling of wind turbine wakes 2002 *Journal of Fluids Engineering* **124** 393–399
[19] Joulin P A, Mayol M L, Masson V, Blondel F, Rodier Q, Cathelain M and Lac C The actuator line method in the meteorological LES model meso-NH to analyze the horns rev 1 wind farm photo case 2020 *Frontiers in Earth Science* **7**
[20] Stein J, Richard E, Lafore J P, Pinty J P, Asencio N and Cosma S High-resolution non-hydrostatic simulations of flash-flood episodes with grid-nesting and ice-phase parameterization 2000 *Meteorology and Atmospheric Physics* **72** 203–221
[21] Troldborg N 2009 *Actuator Line Modeling of Wind Turbine Wakes* PhD Thesis
[22] Stevens R J, Martínez-Tossas L A and Meneveau C Comparison of wind farm large eddy simulations using actuator disk and actuator line models with wind tunnel experiments 2018 *Renewable Energy* **116** 470–478
[23] Vollmer L, Steinfeld G, Heinemann D and Kühn M Estimating the wake deflection downstream of a wind turbine in different atmospheric stabilities: an LES study 2016 *Wind Energy Science* **1** 129–141
[24] Quon E W, Doubrawa P and Debnath M Comparison of rotor wake identification and characterization methods for the analysis of wake dynamics and evolution 2020 *Journal of Physics: Conference Series* **1452** 012070
[25] Doubrawa P, Martínez-Tossas L A, Quon E, Moriarty P and Churchfield M J Comparison of mean and dynamic wake characteristics between research-scale and full-scale wind turbines 2018 *Journal of Physics: Conference Series* **1037** 072053 URL `https://doi.org/10.1088/1742-6596/1037/7/072053`
[26] Ning X and Wan D LES study of wake meandering in different atmospheric stabilities and its effects on wind turbine aerodynamics 2019 *Sustainability* **11** 6939
[27] Aubrun S, Muller Y A and Masson C Predicting wake meandering in real-time through instantaneous measurements of wind turbine load fluctuations 2015 *Journal of Physics: Conference Series* **625** 012005
[28] Abkar M, Sørensen J and Porté-Agel F An Analytical Model for the Effect of Vertical Wind Veer on Wind Turbine Wakes 2018 *Energies* **11** 1838
[29] Englberger A, Dörnbrack A and Lundquist J K Does the rotational direction of a wind turbine impact the wake in a stably stratified atmospheric boundary layer? 2020 *Wind Energy Science* **5** 1359–1374